Letter

Transverse momentum resolved angular streaking after tunneling ionization

Dianxiang Ren,[1,2,*] Chao Chen,[3,4,*] Xiaokai Li,[1,2] Xiaoge Zhao,[1,2] Shang Wang,[3,5] Mingxuan Li,[1,2] Xinning Zhao,[1,2] Pan Ma,[1,2] Chuncheng Wang,[1,2] Yujun Yang,[1,2] Yanjun Chen,[3] Sizuo Luo,[1,2,†] and Dajun Ding[1,2,‡]

[1]*Institute of Atomic and Molecular Physics, Jilin University, Changchun 130012, China*

[2]*Jilin Provincial Key Laboratory of Applied Atomic and Molecular Spectroscopy, Jilin University, Changchun 130012, China*

[3]*College of Physics and Information Technology, Shaan'xi Normal University, Xi'an 710119, China*

[4]*College of Physics and Electronic Engineering, Xingtai University, Xingtai 054001, China*

[5]*College of Physics and Hebei Key Laboratory of Photophysics Research and Application, Hebei Normal University, Shijiazhuang 050024, China*

(Received 29 March 2023; revised 30 June 2023; accepted 22 August 2023; published 25 September 2023)

The initial momentum along laser propagation plays a significant role in the electron dynamics during tunneling ionization. Our study shows that the offset emission angle decreases with increasing lateral momentum. By using three-dimensional strong-field approximation calculations with initial transverse momentum and a Coulomb correction, we accurately reproduce the transverse momentum-dependent angular shifts of Ar, Kr, and Xe atoms. We find that these shifts are attributed to the influence of initial momentum, tunneling exits, and a long-range Coulomb potential during electron propagation. Additionally, we establish a formula to reconstruct the initial transverse momentum from the final transverse momentum. The result may provide another perspective on attosecond angular streaking, which is crucial for understanding the influence of the Coulomb potential on electron motion.

DOI: 10.1103/PhysRevResearch.5.L032044

The angular streaking technique utilizes an elliptically polarized laser field to map the temporal information of photoelectrons onto their angular spatial distribution. One crucial aspect of this method is the establishment of a temporal-angular connection [1–5]. The vectors of the laser field serve as hands on a clock, with the major axis of the polarization serving as the time zero reference in strong-field angular streaking (attoclock) [1,2]. Alternatively, combined linear extreme ultraviolet (XUV) and circular infrared (IR) pulses can also be used to extract the delay time by setting the polarization direction of the XUV as the time zero reference [6,7]. In cases where the XUV and IR delays are unstable, self-referenced attosecond streaking has been developed [6,7]. Therefore, the angular streaking method has also been utilized for reconstructing the pulse duration of attosecond pulses [6–9], clocking the delay time between the Auger electron and photoelectrons [10], and tracing the coherent electron motion from molecular Auger-Meitner decay [11]. In the strong-field physics, the most probable emission angle of a photoelectron relative to the instants of the field maximum can be resolved with attosecond time resolution. This provides valuable insights into measuring the tunneling time [4,12,13] and Wigner delays [2,5,14], studying the nonadiabatic effects [15–17], and performing initial state reconstructions [14]. The accuracy of extracting temporal information is limited by fully evaluating the phase of the electron wave packet accumulated when propagating out of the Coulomb potential [18].

Recent research has made significant progress in understanding the influence of initial momentum on strong-field tunneling ionization [15,16,19]. During tunneling ionization, the electron gains momentum from the combined effects of the laser field and Coulomb potential. The instantaneous negative vector potential determines the amount of momentum added to the initial momentum in the polarization plane at the tunnel exit. However, obtaining a simple relationship between the final and initial momentum is difficult, as the laser field and Coulomb potential both contribute to the final electron momentum [16,20,21]. Previous angular streaking experiments have focused on integrating photoelectron momentum distributions (PMDs) over transverse momentum and ignoring its impact on emission directions [1,2,4,20]. Nonetheless, the transverse momentum information has recently drawn considerable interest in the strong-field community. Electron dynamics along the laser propagation direction are critical in studying nonadiabatic [17,22], nondipole [23–25], and Coulomb focusing [17,26–30], and even provides zeptosecond time resolution information [31]. Since transverse momentum directly correlates with the Coulomb potential, the anisotropic molecular orbital can be extracted from the transverse momentum slice of electrons [32–35]. The application of this information to the study of electron ionization dynamics in chiral molecules is becoming increasingly interesting [36,37]. Unlike the polarization plane, there is no laser field in

*These authors contributed equally to this work.

†Corresponding author: luosz@jlu.edu.cn.

‡Corresponding author: dajund@jlu.edu.cn

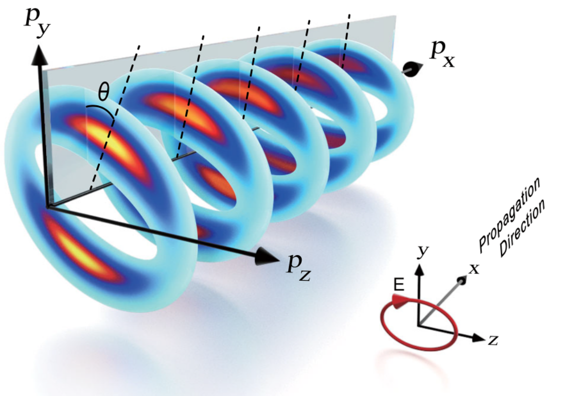

FIG. 1. Schematic diagram of electron momentum distributions with different transverse momenta from strong-field tunneling ionization. θ, the offset angle between the most-probable emission direction and the minor axis y of the laser ellipse.

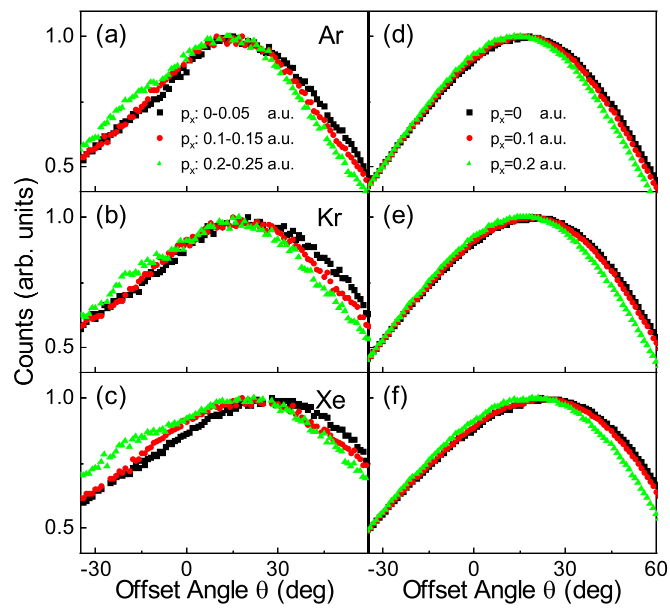

FIG. 2. (a)–(c) show the measured angular distributions of photoelectrons from Ar, Kr, and Xe atoms at three transverse momenta p_x. (d)–(f) present the corresponding SCTS simulated results.

the propagation direction. As a result, it is possible to retrieve the initial transverse momentum of the electron along the laser propagation direction.

In this Letter, we systematically examine the PMDs of noble gas atoms (Ar, Kr, and Xe) in an intense elliptically polarized laser pulse to evaluate the influence of initial transverse momentum distribution. We collect the three-dimensional (3D) photoelectron momentum in a cold target recoil ion spectrometer (COLTRIMS) [38,39]. A 35-fs laser centered at 800 nm passes through a quarter-wave ($\lambda/4$) plate and a half-wave ($\lambda/2$) plate and then is focused onto a mixture gas of Ar, Kr, and Xe atoms by a 75-mm concave mirror, with a laser intensity of $I \sim 1.6 \times 10^{14}$ W/cm^2 and an ellipticity of $\varepsilon = 0.8$. The electron momenta for three atoms are collected simultaneously to retain absolutely identical laser and experimental parameters, and the PMDs of three species are separated unambiguously by ion tagging. By slicing PMDs with varying transverse momenta under the same conditions, it is possible to directly compare and extract Coulomb effects for different targets with different initial transverse momenta. Figure 1 displays the transverse momentum resolved 3D PMDs, from which the offset angles are extracted to track the electron dynamics.

Theoretically, we analyze the emission angles of the PMDs using a semiclassical two-step (SCTS) [15] model that includes a Coulomb interaction after tunneling [see Supplemental Material (SM) [40] for details]. By solving the saddle-point equation [41]

$$[\mathbf{p} + \mathbf{A}(t_s)]^2/2 + I_p = 0, \tag{1}$$

the corresponding tunneling amplitude $F(\mathbf{p}, t_s)$ for the trajectory $(\mathbf{p}, t_s)$ can be written as

$$F(\mathbf{p}, t_s) \propto \sum_s \gamma \mathbf{E}(t_s) \cdot \mathbf{d}_i[\mathbf{p} + \mathbf{A}(t_s)]e^{iS(\mathbf{p},t_s)}, \tag{2}$$

where $S(\mathbf{p}, t_s) = \int^{t_s}\{[\mathbf{p} + \mathbf{A}(t')]^2/2 + I_p\}dt'$ is the semiclassical action and $\gamma = [1/\det(t_s)]^{1/2}$. The index s runs over the relevant saddle points, which are also termed as quantum orbits. After tunneling, the 3D electron motion in the combined laser and Coulomb field is governed by the Newtonian equation [42]

$$\ddot{\mathbf{r}}(\mathbf{p}, t) = -\mathbf{E}(t) - \nabla_{\mathbf{r}} V(\mathbf{r}), \tag{3}$$

with $V(\mathbf{r}) = Z_e e^{-\rho r}/\sqrt{x^2 + y^2 + z^2}$. The screening parameter $\rho = 0$ for the long-range Coulomb potential (LRP) and the parameters ρ for Ar, Kr, and Xe atoms are 0.5, 0.48, and 0.44 a.u. for the short-range potential (SRP) case. $Z_e = \sqrt{2I_p}$ is the effective charge. For each trajectory, the initial momentum is $\dot{\mathbf{r}}(\mathbf{p}, t_s^r) = \mathbf{p} + \mathbf{A}(t_s^r)$ and the exiting position can be determined by $\mathbf{r}(\mathbf{p}, t_s^r) = \mathrm{Re}\int_{t_s}^{t_s^r}[\mathbf{p} + \mathbf{A}(t')]dt'$, t_s^r is the real part of the saddle-point time t_s which is considered as the time of the electron tunneling through the laser-Coulomb barrier. The Newton equation Eq. (3) is solved using the Runge-Kutta method with adaptive step-size control. Then, the final Coulomb-modified drift momentum is obtained with $\mathbf{p}' = \dot{\mathbf{r}}(\mathbf{p}, t_\infty)$. Compared to the 2D case, Eq. (3) includes the electron's motion along the laser propagation direction, leading to a weakening of the Coulomb effect and a reduction of the offset angles of PMDs (see SM [40] for the measured and simulated PMDs).

Figures 2(a)–2(c) display the measured photoelectron angular distributions from Ar, Kr, and Xe atoms at three transverse momenta p_x, with the signals projected onto the $p_y p_z$ plane. The data were selected for each p_x using a uniform increment of $\Delta p_x = 0.05$ a.u. Figures 2(d)–2(f) present the results obtained from SCTS. Both the experimental and SCTS results indicate a decrease in the offset emission angles as the final transverse momentum increases.

To compare the offset angles, we present the dependence of the offset angles to the final transverse momenta in Fig. 3(a). Here, LRP and experiment results show the same tendency, and the offset angle decreases as transverse momentum increases. The simulated results from SRP give a almost zero angular offset for all p_x, indicating that the changing of offset

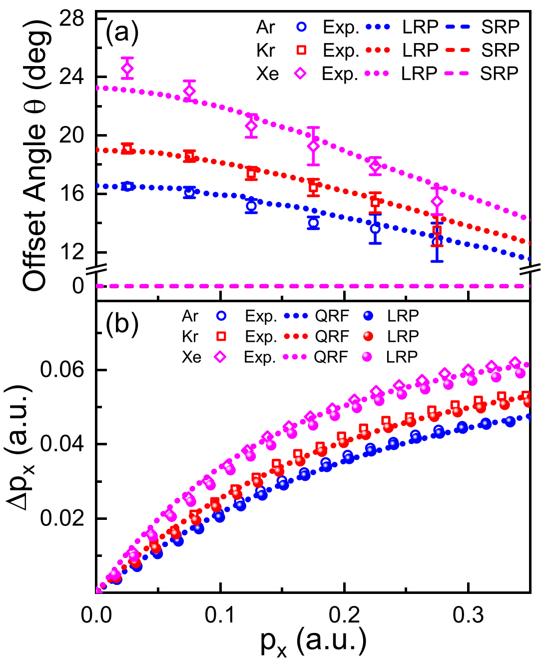

FIG. 3. (a) The measured and calculated offset angles as a function of the final transverse momentum p_x for Ar, Kr, and Xe atoms. (b) The measured Δp_x as a function of p_x for three noble gas atoms are represented by open symbols. The QRF predicted curves are represented by a dotted-dashed line and the SCTS simulations with LRP are shown by spherical symbols.

angles with the transverse momentum p_x originates from the long-range Coulomb interaction during the propagation [12]. Under the same laser conditions, the results from Xe atoms have a stronger dependence than the Ar atoms. This can be explained by the fact that the tunnel exit of the Xe atoms is closer than that of the Ar atoms [17].

It is worthwhile to note that when transverse momentum is integrated, the resulting angular shift is significantly lower than that obtained using a 2D cutting approach ($p_x \leqslant 0.05$ a.u.). The difference is approximately 2°–4° corresponding to a delay of 15–30 attoseconds for three atoms, indicating that the 2D tunneling model overestimates the angular shift compared to the actual 3D electron dynamics. Thus, to accurately study strong-field angular streaking, it is important to consider the electron dynamics in the laser propagation direction.

The dependence of the transverse momentum on the offset angles can be further discussed by a SCTS model, which incorporates the initial transverse momentum p_x^0 and 3D Coulomb interaction after tunneling. The classical propagation after tunneling leads to a nonzero offset angle of the photoelectron angular distributions in the laser polarization plane, and the offset angle is directly related to the position of the tunnel exit [16]. The tunnel exit is closer to the core for a smaller ionization potential under the same laser intensity, thus the Coulomb potential has a stronger influence on the released electron wave packet. As a result, the offset angle for Xe atoms is large for small transverse momentum p_x, as shown in Fig. 3(a). For three atoms, as the transverse momentum increases, the accumulation of Coulomb effects increases along the laser propagation direction, leading to a gradual reduction of the difference in the offset angles. Meanwhile, the offset angle tends to be the same when the transverse momentum increases to the region of $p_x > 0.3$ a.u.

In the laser propagation direction, electrons are not affected by the laser field, but only by the Coulomb interaction of the core. A one-to-one correspondence can therefore be established between the final momentum and the initial momentum, that is, a greater initial momentum corresponds to a greater final momentum. Thus, one can reconstruct the initial transverse momentum distribution accordingly. Although the laser fields are absent along the propagation direction, it is still difficult to analytically establish a quantitative relationship between the initial and final transverse momentum, because the motion of the electrons in the oscillating laser fields and the Coulomb potential along the laser propagation direction are coupled within the polarization plane, which also induces a shift of the emission angles. To retrieve the initial transverse momentum directly, a quantitative reconstruction formula (QRF) between the final momentum p_x and initial momentum p_x^0 is established,

$$\Delta p_x = -A(e^{-p_x/\sigma} - 1). \tag{4}$$

Here, $\Delta p_x = p_x^0 - p_x$ represents the momentum reduction along the laser propagation under the Coulomb interaction after tunneling. A and σ give the response of the Coulomb potential along laser propagation after tunneling, and are related to the ionization potential and laser intensity. The fitting curves based on this formula are shown in Fig. 3(b). Based on the agreement of the measured offset angles as shown in Fig. 3(a), the initial momentum is obtained from the SCTS calculation, whereas the final transverse momentum is obtained from measurement (see SM [40]). Both the results from the experiment and SCTS calculation show that Xe atoms have a larger Δp_x comparing to the Ar and Kr atoms, due to the fact that the tunnel exit of Xe atoms is closer to the core in the polarization plane. Now, utilizing this formula, we can build the relations between Δp_x and the ionization potential as well as the laser intensity directly.

Based on the agreements achieved in Figs. 2 and 3, the parameters A and σ in Eq. (4) are extracted from the best fit of the Δp_x data at different laser intensities and atoms with artificial ionization potentials (see SM [40] for more simulation results). Thus, A and σ are written as

$$A = k(I_p)(I + \alpha) + \beta \tag{5}$$

and

$$\sigma = \zeta I_p - \eta(E_0), \tag{6}$$

for which the dependence is shown in Figs. 4(a) and 4(c). A similar role has been found for probing the tunnel exit [20]. In the above expressions, $k(I_p) = 0.001\,95 I_p^{-3/2}$ is related to the ionization potential and $\eta(E_0) = 0.048(E_0/0.0548 + 1)$ is a linear function with the field strength as shown in Figs. 4(b) and 4(d). Here, E_0 is the amplitude of the laser field. In Fig. 4, the parameters labeled as "Exp." are obtained from best fitting of the experimental data of Fig. 3(b). Here, $\alpha = 2.1$, $\beta = 0.044$, and $\zeta = 0.591\,95$ are the constant factors. The formula presented in Eq. (4) can be extended to include additional atomic and molecular targets and laser conditions (see SM [40] for the validation). Moreover, the influence of the

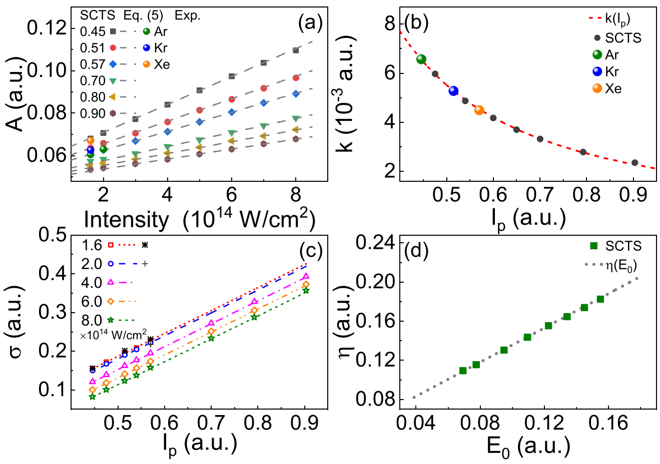

FIG. 4. (a) The parameter A with respect to the laser intensity for different ionization potentials. (b) The parameter k as a function of the ionization potential extracted from the intensity dependence of parameter A. (c) The parameter σ as a function of the ionization potential for different laser intensities. (d) The parameter η as a function of external field E_0 extracted from Eq. (6).

ionization potential and laser intensity on Δp_x is opposite. As the ionization potential decreases, the electron's tunnel exit moves closer to the core, leading to a larger Δp_x. On the other hand, decreasing the laser intensity causes the tunnel exit to move away from the core, resulting in a smaller Δp_x. The derived equations offer a straightforward method to calculate the initial momentum of an electron from its final distribution, which provide a protocol to quantitatively assess the influence of ionization potential and laser intensity on the electron dynamics.

In order to delve deeper into the impact of wavelength on the distribution of transverse momentum resulting from tunneling ionization, we have conducted calculations on the electron distribution arising from the tunneling ionization of an Ar atom using a laser with wavelengths of 800, 1000, and 1300 nm. Figure 5 presents the relationship between Δp_x and the final transverse momentum p_x for each of these wavelengths, all while maintaining the same laser intensity ($I = 2 \times 10^{14}$ W/cm^2). These insights are garnered from computations within the SCTS, revealing a trend where increasing the wavelength leads to a reduction in Δp_x for a given p_x. This observation underscores the significant influence of nonadiabatic effects on the transverse momentum, as governed by the laser wavelength. Importantly, the QRF method demonstrates effectiveness across these three wavelengths. This behavior

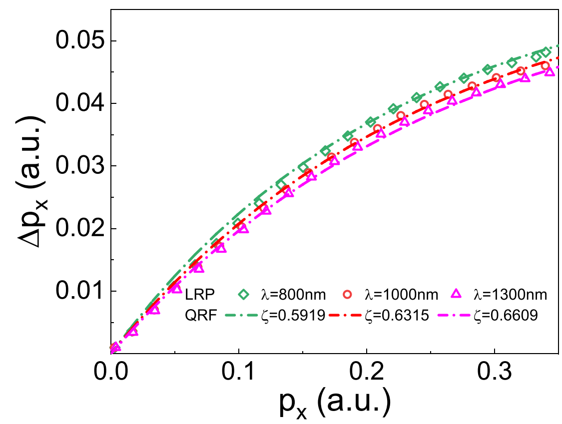

FIG. 5. The dependence of Δp_x on the final transverse momentum p_x for different laser wavelengths. The predictions of QRF are depicted as short dotted lines, while the results of the SCTS simulation are represented by symbols.

can be accurately characterized by fine tuning the constant ζ within Eq. (6). The agreement between theoretical and empirical results accentuates the potential utility of the QRF approach, coupled with the angular streaking measurement of transverse momentum, in exploring the tunneling ionization dynamics within a nonadiabatic condition.

In conclusion, the transverse momentum resolved photoionization of Ar, Kr, and Xe atoms, under strong laser fields has been studied by angular streaking. Three-dimensional SCTS simulations have confirmed that electron emission angles decrease as transverse momentum increases for all three atoms. The measured shifts in the electron emission angles are attributed to the long-range Coulomb potential and initial momentum during electron propagation. We have summarized formulas that can evaluate the impact of the Coulomb potential and laser field, and also reconstructed the initial transverse momentum from the final measured transverse momentum. These shifts have been observed in different atomic and molecular systems, providing valuable information on the laser modification Coulomb potential and allowing for the tracking of electron dynamics in chiral molecules after tunneling ionization.

This work was supported by the National Natural Science Foundation of China (Grants No. 12134005, No. 92250306, No. 12004135, and No. 12174239), and the National Basic Research Program of China (Grant No. 2019YFA0307701).

[1] P. Eckle, A. N. Pfeiffer, C. Cirelli, A. Staudte, R. Dörner, H. G. Muller, M. Büttiker, and U. Keller, Attosecond ionization and tunneling delay time measurements in helium, Science **322**, 1525 (2008).

[2] U. S. Sainadh, H. Xu, X. Wang, A. Atia-Tul-Noor, W. C. Wallace, N. Douguet, A. Bray, I. Ivanov, K. Bartschat, A. Kheifets, R. T. Sang, and I. V. Litvinyuk, Attosecond angular streaking and tunnelling time in atomic hydrogen, Nature (London) **568**, 75 (2019).

[3] S. Eckart, M. Kunitski, M. Richter, A. Hartung, J. Rist, F. Trinter, K. Fehre, N. Schlott, K. Henrichs, L. P. H. Schmidt, T. Jahnke, M. Schöffler, K. Liu, I. Barth, J. Kaushal, F. Morales, M. Ivanov, O. Smirnova, and R. Dörner, Ultrafast preparation and detection of ring currents in single atoms, Nat. Phys. **14**, 701 (2018).

[4] N. Camus, E. Yakaboylu, L. Fechner, M. Klaiber, M. Laux, Y. Mi, K. Z. Hatsagortsyan, T. Pfeifer, C. H. Keitel, and R. Moshammer, Experimental Evidence for

Quantum Tunneling Time, Phys. Rev. Lett. **119**, 023201 (2017).

[5] A. N. Pfeiffer, C. Cirelli, M. Smolarski, D. Dimitrovski, M. Abu-samha, L. B. Madsen, and U. Keller, Attoclock reveals natural coordinates of the laser-induced tunnelling current flow in atoms, Nat. Phys. **8**, 76 (2012).

[6] N. Hartmann, R. H. G. Hartmann, M. S. Wagner, M. Ilchen, J. Buck, C. B. A. O. Lindahl, J. Grünert, J. Krzywinski, J. Liu, A. A. Lutman, A. Marinelli, T. Maxwell, A. A. Miahnahri, S. P. Moeller, M. Planas, J. Robinson, A. K. Kazansky, N. M. Kabachnik, J. Viefhaus, T. Feurer *et al.*, Attosecond time-energy structure of x-ray free-electron laser pulses, Nat. Photonics **12**, 215 (2018).

[7] J. Duris, S. Li, T. Driver, E. G. Champenois, J. P. MacArthur, A. A. Lutman, Z. Zhang, P. Rosenberger, J. W. Aldrich, R. Coffee, G. Coslovich, F.-J. Decker, J. M. Glownia, G. Hartmann, W. Helml, A. Kamalov, J. Knurr, J. Krzywinski, M.-F. Lin, J. P. Marangos *et al.*, Tunable isolated attosecond x-ray pulses with gigawatt peak power from a free-electron laser, Nat. Photonics **14**, 30 (2020).

[8] Z. X. Zhao, Z. Chang, X. M. Tong, and C. D. Lin, Circularly-polarized laser-assisted photoionization spectra of argon for attosecond pulse measurements, Opt. Express **13**, 1966 (2005).

[9] X. Zhao, S. Li, T. Driver, V.-H. Hoang, A.-T. Le, J. P. Cryan, A. Marinelli, and C. D. Lin, Characterization of single-shot attosecond pulses with angular streaking photoelectron spectra, Phys. Rev. A **105**, 013111 (2022).

[10] T. Uphues, M. Schultze, M. F. Kling, M. Uiberacker, S. Hendel, U. Heinzmann, N. M. Kabachnik, and M. Drescher, Ion-charge-state chronoscopy of cascaded atomic Auger decay, New J. Phys. **10**, 025009 (2008).

[11] D. C. Haynes, M. Wurzer, A. Schletter, A. Al-Haddad, C. Blaga, C. Bostedt, J. Bozek, H. Bromberger, M. Bucher, A. Camper, S. Carron, R. Coffee, J. T. Costello, L. F. DiMauro, Y. Ding, K. Ferguson, I. Grguraš, W. Helml, M. C. Hoffmann, M. Ilchen *et al.*, Clocking Auger electrons, Nat. Phys. **17**, 512 (2021).

[12] L. Torlina, F. Morales, J. Kaushal, I. Ivanov, A. Kheifets, A. Zielinski, A. Scrinzi, H. G. Muller, S. Sukiasyan, M. Ivanov, and O. Smirnova, Interpreting attoclock measurements of tunnelling times, Nat. Phys. **11**, 503 (2015).

[13] H. Ni, U. Saalmann, and J.-M. Rost, Tunneling Ionization Time Resolved by Backpropagation, Phys. Rev. Lett. **117**, 023002 (2016).

[14] I. Babushkin, Á. J. Galán, J. R. C. de Andrade, A. Husakou, F. Morales, M. Kretschmar, T. Nagy, V. Vaičaitis, L. Shi, D. Zuber, L. Bergé, S. Skupin, I. A. Nikolaeva, N. A. Panov, D. E. Shipilo, O. G. Kosareva, A. N. Pfeiffer, A. Demircan, M. J. J. Vrakking, U. Morgner *et al.*, All-optical attoclock for imaging tunnelling wavepackets, Nat. Phys. **18**, 417 (2022).

[15] D. Trabert, N. Anders, S. Brennecke, M. S. Schöffler, T. Jahnke, L. P. H. Schmidt, M. Kunitski, M. Lein, R. Dörner, and S. Eckart, Nonadiabatic Strong Field Ionization of Atomic Hydrogen, Phys. Rev. Lett. **127**, 273201 (2021).

[16] R. Boge, C. Cirelli, A. S. Landsman, S. Heuser, A. Ludwig, J. Maurer, M. Weger, L. Gallmann, and U. Keller, Probing Nonadiabatic Effects in Strong-Field Tunnel Ionization, Phys. Rev. Lett. **111**, 103003 (2013).

[17] M. Li, Y. Liu, H. Liu, Q. Ning, L. Fu, J. Liu, Y. Deng, C. Wu, L.-Y. Peng, and Q. Gong, Subcycle Dynamics of Coulomb Asymmetry in Strong Elliptical Laser Fields, Phys. Rev. Lett. **111**, 023006 (2013).

[18] M. Ivanov and O. Smirnova, How Accurate Is the Attosecond Streak Camera? Phys. Rev. Lett. **107**, 213605 (2011).

[19] S. P. Goreslavski, G. G. Paulus, S. V. Popruzhenko, and N. I. Shvetsov-Shilovski, Coulomb Asymmetry in Above-Threshold Ionization, Phys. Rev. Lett. **93**, 233002 (2004).

[20] A. S. Landsman, C. Hofmann, A. N. Pfeiffer, C. Cirelli, and U. Keller, Unified Approach to Probing Coulomb Effects in Tunnel Ionization for Any Ellipticity of Laser Light, Phys. Rev. Lett. **111**, 263001 (2013).

[21] S. Brennecke, S. Eckart, and M. Lein, Attoclock with bicircular laser fields as a probe of velocity-dependent tunnel-exit positions, J. Phys. B: At., Mol. Opt. Phys. **54**, 164001 (2021).

[22] S. Eckart, K. Fehre, N. Eicke, A. Hartung, J. Rist, D. Trabert, N. Strenger, A. Pier, L. Ph. H. Schmidt, T. Jahnke, M. S. Schöffler, M. Lein, M. Kunitski, and R. Dörner, Direct Experimental Access to the Nonadiabatic Initial Momentum Offset upon Tunnel Ionization, Phys. Rev. Lett. **121**, 163202 (2018).

[23] K. Lin, X. Chen, S. Eckart, H. Jiang, A. Hartung, D. Trabert, K. Fehre, J. Rist, L. Ph. H. Schmidt, M. S. Schöffler, T. Jahnke, M. Kunitski, F. He, and R. Dörner, Magnetic-Field Effect as a Tool to Investigate Electron Correlation in Strong-Field Ionization, Phys. Rev. Lett. **128**, 113201 (2022).

[24] B. Willenberg, J. Maurer, B. W. Mayer, and U. Keller, Sub-cycle time resolution of multi-photon momentum transfer in strong-field ionization, Nat. Commun. **10**, 5548 (2019).

[25] H. Ni, S. Brennecke, X. Gao, P.-L. He, S. Donsa, I. Brezinova, F. He, J. Wu, M. Lein, X.-M. Tong, and J. Burgdorfer, Theory of Subcycle Linear Momentum Transfer in Strong-Field Tunneling Ionization, Phys. Rev. Lett. **125**, 073202 (2020).

[26] J. Daněk, K. Z. Hatsagortsyan, and C. H. Keitel, Analytical approach to Coulomb focusing in strong-field ionization. I. Nondipole effects, Phys. Rev. A **97**, 063409 (2018).

[27] D. Comtois, D. Zeidler, H. Pépin, J. C. Kieffer, D. M. Villeneuve, and P. B. Corkum, Observation of Coulomb focusing in tunnelling ionization of noble gases, J. Phys. B: At., Mol. Opt. Phys. **38**, 1923 (2005).

[28] D. Shafir, H. Soifer, C. Vozzi, A. S. Johnson, A. Hartung, Z. Dube, D. M. Villeneuve, P. B. Corkum, N. Dudovich, and A. Staudte, Trajectory-Resolved Coulomb Focusing in Tunnel Ionization of Atoms with Intense, Elliptically Polarized Laser Pulses, Phys. Rev. Lett. **111**, 023005 (2013).

[29] X. Huang, Q. Zhang, S. Xu, X. Fu, X. Han, W. Cao, and P. Lu, Coulomb focusing in retrapped ionization with near-circularly polarized laser field, Opt. Express **27**, 38116 (2019).

[30] T. Brabec, M. Y. Ivanov, and P. B. Corkum, Coulomb focusing in intense field atomic processes, Phys. Rev. A **54**, R2551 (1996).

[31] S. Grundmann, D. Trabert, K. Fehre, N. Strenger, A. Pier, L. Kaiser, M. Kircher, M. Weller, S. Eckart, L. P. H. Schmidt, F. Trinter, T. Jahnke, M. S. Schöffler, and R. Dörner, Zeptosecond birth time delay in molecular photoionization, Science **370**, 339 (2020).

[32] J. Maurer, D. Dimitrovski, L. Christensen, L. B. Madsen, and H. Stapelfeldt, Molecular-Frame 3D Photoelectron Momentum Distributions by Tomographic Reconstruction, Phys. Rev. Lett. **109**, 123001 (2012).

[33] D. Dimitrovski, J. Maurer, H. Stapelfeldt, and L. B. Madsen, Low-Energy Photoelectrons in Strong-Field Ionization by Laser Pulses with Large Ellipticity, Phys. Rev. Lett. **113**, 103005 (2014).

[34] I. Petersen, J. Henkel, and M. Lein, Signatures of Molecular Orbital Structure in Lateral Electron Momentum Distributions from Strong-Field Ionization, Phys. Rev. Lett. **114**, 103004 (2015).

[35] X. Zhao, T. Xu, X. Yu, D. Ren, M. Li, X. Zhang, X. Li, P. Ma, D. Zhang, C. Wang, Q. Wang, X. Hu, Y. Wu, J. Wang, and D. Ding, Probing electron localization during molecular dissociation by femtosecond strong-field ion momentum spectroscopy, Commun. Phys. **6**, 124 (2023).

[36] E. Kutscher, A. N. Artemyev, and P. V. Demekhin, Photoelectron circular dichroism in fenchone by short coherent broadband laser pulses, Phys. Rev. A **107**, 013107 (2023).

[37] K. Fehre, S. Eckart, M. Kunitski, C. Janke, D. Trabert, J. Rist, M. Weller, A. Hartung, M. Pitzer, L. Ph. H. Schmidt, T. Jahnke, R. Dörner, and M. S. Schöffler, Angular streaking in strong field ionization of chiral molecules, Phys. Rev. Res. **1**, 033045 (2019).

[38] R. Dörner, V. Mergel, O. Jagutzki, L. Spielberger, J. Ullrich, R. Moshammer, and H. Schmidt-Böcking, Cold target recoil ion momentum spectroscopy: a 'momentum microscope' to view atomic collision dynamics, Phys. Rep. **330**, 95 (2000).

[39] J. Ullrich, R. Moshammer, A. Dorn, R. Dörner, L. P. H. Schmidt, and H. Schmidt-Böcking, Recoil-ion and electron momentum spectroscopy: reaction-microscopes, Rep. Prog. Phys. **66**, 1463 (2003).

[40] See Supplemental Material at http://link.aps.org/supplemental/10.1103/PhysRevResearch.5.L032044 for detailed theoretical methods, and additional experimental and theoretical results.

[41] M. Lewenstein, P. Balcou, M. Y. Ivanov, A. L'Huillier, and P. B. Corkum, Theory of high-harmonic generation by low-frequency laser fields, Phys. Rev. A **49**, 2117 (1994).

[42] T.-M. Yan, S. V. Popruzhenko, M. J. J. Vrakking, and D. Bauer, Low-Energy Structures in Strong Field Ionization Revealed by Quantum Orbits, Phys. Rev. Lett. **105**, 253002 (2010).